Effects of Filler Type on the Nonisothermal Crystallization Kinetics of Poly(butylene terephthalate) (PBT) Composites

Nur Oburoğlu, Nevra Ercan, Ali Durmus, Ahmet Kaşgöz

Department of Chemical Engineering, Faculty of Engineering, Istanbul University, 34320, Avcilar, Istanbul, Turkey

Received 29 January 2011; accepted 28 February 2011
DOI 10.1002/app.34464
Published online 25 July 2011 in Wiley Online Library (wileyonlinelibrary.com).

ABSTRACT: In this study, melt-crystallization behaviors of poly(butylene terephthalate) (PBT) composites including different types of inorganic fillers were investigated. Composite samples having 5 wt % of fillers were prepared by melt processing in a twin screw extruder using commercial grades of calcite (CA), halloysite (HL), and organo-montmorillonite (OM) as filler. Depending on the filler type and geometry, crystallization kinetics of the samples was studied by differential scanning calorimetry (DSC) methods. Effect of filler type on the nonisothermal melt-crystallization kinetics of the PBT was analyzed with various kinetic models, namely, the Ozawa, Avrami modified by Jeziorny and Liu-Mo. Crystallization activation energies of the samples were also determined by the Kissinger, Takhor, and Augis–Bennett models. From the kinetics study, it was found that the melt-crystallization rates of the samples including CA and HL-nanotube were higher than PBT at a given cooling rate. On the other hand, it was also found that organo-montmorillonite reduced the melt-crystallization rate of PBT. It can be concluded that organic ammonium groups in the OM decelerate the crystallization rate of PBT chains possibly due to affecting the chain diffusion through growing crystal face and folding. This study shows that introducing organically modified alumina-silicate layers into the PBT-based composites could significantly reduce the production rate of the injection molded parts during the processing operations. © 2011 Wiley Periodicals, Inc. J Appl Polym Sci 123: 77–91, 2012

Key words: polyesters; composites; crystallization; differential scanning calorimetry

INTRODUCTION

Poly(butylene terephthalate) (PBT), one of the most widely used semicrystalline thermoplastics polyesters, has many applications in various application areas of engineering materials due to its superior thermal and mechanical properties and excellent dimensional stability. PBT exhibits two different crystal structures, the α- and β-forms which both with a triclinic unit crystal cell. β-Form crystals develop only under special processing conditions (e.g., application of stress to un-oriented crystals).[1] Furthermore, two different types of spherulites could be formed on PBT crystallization from the melt state, which both has the same crystalline structure (α). It is well known that physical properties of a semicrystalline polymer are governed by the supramolecular structure, which in turn is controlled by the crystallization.

Improved thermal, mechanical, and barrier properties of PBT composites and nanocomposites have been reported so far.[2–6] In recent years, isothermal or nonisothermal crystallization kinetics of PBT blends and composites has also been studied.[7–11] Wu et al.[12] studied the nonisothermal crystallization kinetics of PBT/organo-montmorillonite nanocomposites by differential scanning calorimetry (DSC) method. They reported that small amounts of clay (1 wt %) could accelerate the crystallization process, whereas higher clay loadings reduced the rate of crystallization. Chen et al.[13] studied the isothermal crystallization kinetics of PBT/organo-attapulgite nanocomposites and concluded that the addition of attapulgite did not alter the crystal structure of PBT, whereas accelerated the isothermal crystallization rate of PBT. They also pointed out that organo-attapulgite could behave as a good nucleating agent for the crystallization of PBT by reducing fold surface free energy during the crystallization but it could also restrict the segmental motion of PBT. Al-Mulla et al.[14] investigated the nonisothermal crystallization kinetics of PBT, PBT/nanoclay, and PBT/carbon nanofiber composites. Li et al.[4] studied the effects of nano-TiO_2 and surface-modified nano-TiO_2 on the impact properties and crystallization behavior of PBT.

To the best of our knowledge, a comprehensive study has not been published yet to understand the effects of filler type and geometry on the

Correspondence to: N. Ercan (n.ercan@isnet.net.tr).
Contract grant sponsor: This study was supported by the Research Fund of Istanbul University; contract grant number: 2386.

© 2011 Wiley Periodicals, Inc.

TABLE I
Some Physical Properties of the Fillers

Physical property	Fillers		
	Calcite ($CaCO_3$)	Halloysite	Organo-montmorillonite
Particle geometry	Spherical (3D)	Nanotube (1D)	Layered (2D)
Commercial name	Filmplus®	Aldrich 685445	Cloisite® 15A
Average particle size	<7.8 μm (%97)	*D*: 30 nm and *L*: 0.25–4 μm	<13 μm (%90)
[a]CEC (meq g^{-1})		0.8	1.25
Density (g cm^{-3})	2.70	2.53	1.66
Surface area (m^2 g^{-1})		64	
Loss of ignition (%)			43
Organic surface modifier	+	−	+

[a] Cation exchange capacity.

crystallization behavior and kinetics of PBT. In this study, nonisothermal crystallization behaviors of PBT-based composites including 5 wt % of micro-size spherical [calcite (CA)], nanosize tubular [halloysite (HL)], and nanosize layered [organo-montmorillonite (OM)] inorganic fillers were studied by DSC method. Effects of filler type and geometry on the nonisothermal melt-crystallization kinetics of PBT were quantitatively compared.

EXPERIMENTAL

Materials

A film grade, amorphous PBT homopolymer (SD85®, intrinsic viscosity value of 0.83 dL/g at 23°C) used in this study was kindly supplied by Advansa, TR. The inorganic fillers were commercially available products. Trade names and physical properties of the fillers are listed in Table I. CA which is a surface coated material was supplied by Mikron'S, Turkey. HL nanotube was ordered from Aldrich. Organo-modified montmorillonite employed in this study (Cloisite® 15A) is dimethyl dehydrogenated tallow quaternary ammonium (2Me2HT) salt-modified clay supplied from Southern Clay, Gonzales, Texas. The organic content of Cloisite® 15A was reported as 43% by the manufacturer.

Sample preparation

Before melt processing, PBT and fillers were dried in a vacuum oven overnight at 80°C. Samples were processed in a lab-scale twin screw extruder (Rondol Micro Lab., UK, *D*: 10 mm, *L*/*D*: 20) with a screw speed of 75 rpm. Screw configuration used for the processing is appeared in Figure 1. A temperature profile of 180–240°C was applied throughout the barrel from feeding zone to die, and then the extrudate was granulated. PBT was also processed under the same conditions. In this study, a sample loading of 5 wt % was preferred for all types of fillers to compare effects of filler type and geometry rather than filler amount on the crystallization behavior of PBT. Sample denotations and compositions are given in Table II.

XRD study

X-ray diffractometer (XRD) analyses were performed with a Rigaku D/Max-2200/PC model (Rigaku, Japan) wide angle XRD with a Cu anode, running at 40 kV and 40 mA, scanning from 2° to 35° at 2° min^{-1}. Analysis was performed with compression molded film samples. Molding conditions were applied as 5 kg cm^{-2} for 1 min and 30 kg cm^{-2} for 2 min at 240°C between Teflon sheets in a hot press. Molded films were cooled to room temperature by water circulation with the cooling rate of $\sim$ 30°C min^{-1}.

DSC study

Melting and crystallization runs were carried out in a heat flow type DSC, Perkin–Elmer, Pyris. Temperature and heat flow calibration of the instrument were achieved with high purity indium (In), tin (Sn), and zinc (Zn) metals. Samples weighing about 6–7 mg in an aluminum crucible were heated from 30 to 250°C with the heating rate of 10°C min^{-1}. Samples were kept at this temperature for 2 min to remove the thermal history then cooled from 250 to 30°C with the cooling rate of 2, 5, 10, and 15°C min^{-1} by liquid nitrogen device of the instrument. After completion of the melt-crystallization process, samples were kept at 30°C for 2 min. Subsequently, nonisothermally crystallized samples at different cooling rates were heated again from the 30 to 250°C with the heating rate of 10°C min^{-1}. Degree of crystallinity (X_c) was determined from the second melting enthalpy values using the following equation:

$$X_c = \frac{\Delta H_m}{(1-\alpha)\Delta H_m^o} \times 100 \quad (1)$$

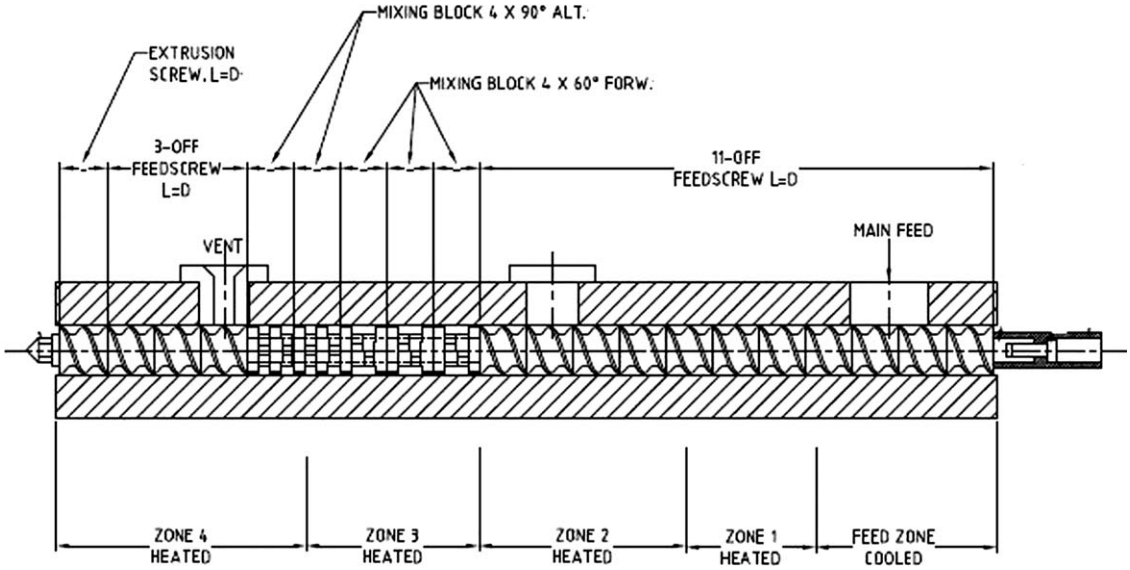

Figure 1 Segmented screw profile used in the lab-scale twin screw extruder.

where ΔH_m is second melting enthalpy of the samples (J g^{-1}), ΔH_m^o is the enthalpy value of melting of a 100% crystalline form of PBT (145.5 J g^{-1}),[15] and α is the weight fraction of filler. All runs were carried out under nitrogen (N_2) atmosphere at a flow rate of 50 mL min^{-1} to prevent thermal degradation of the samples.

RESULTS AND DISCUSSION

XRD results

XRD patterns of the organo-montmorillonite (OM) and PBT–OM samples in the characteristic region for layered alumina-silicates (2θ = 2–10°) are given in Figure 2. Two diffraction peaks are observed for the OM corresponding to basal spacing of d_{001} = 3.07 nm (2θ = 2.88) and d_{002} = 1.21 nm (2θ = 7.31) by using the Bragg equation given as;

$$\lambda = 2dSin\theta \quad (2)$$

where λ is the wavelength of the X-rays (0.154 nm), θ is the diffraction angle, and d is the basal space between clay layers, respectively. d_{001} and d_{002} peaks are also clearly observed for the PBT–OM, but shifted to lower angles which indicate the increasing of the interlamellar distance between clay layers. Visible and shifted peaks suggest that relatively large stacks of clay platelets are still present in the PBT–OM sample showing clay layers being not completely exfoliated. For the PBT–OM, d_{001} and d_{002} values were calculated as 3.62 nm (2θ = 2.44) and 1.87 nm (2θ = 4.73), respectively.

XRD patterns of the PBT and composite samples in the higher diffraction angles which is characteristic for the structure of polymer (2θ = 5–35°) are also given in Figure 3. Comparing the XRD patterns of

TABLE II
Sample Compositions

	wt (%)			
Sample	PBT	Calcite	Halloysite	Organo-montmorillonite
PBT	100			
PBT–CA	95	5		
PBT–HL	95		5	
PBT–OM	95			5

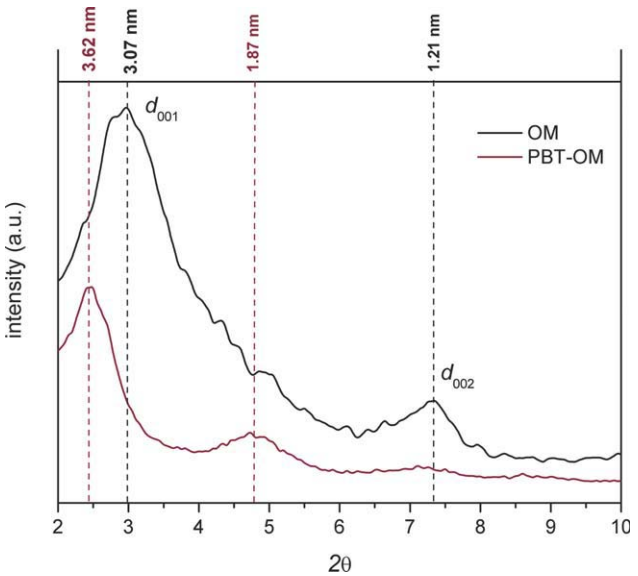

Figure 2 XRD patterns of the organo-montmorillonite and PBT–OM in the characteristic region (2θ = 2–10°) for the state of organo-montmorillonite dispersion. [Color figure can be viewed in the online issue, which is available at wileyonlinelibrary.com.]

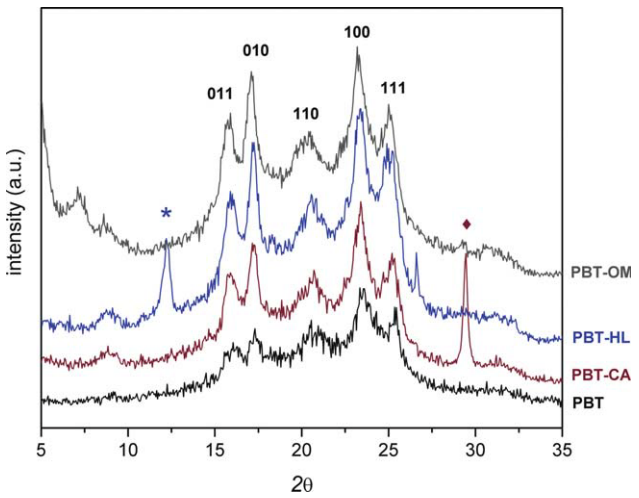

Figure 3 XRD patterns of the PBT and composite samples in the diffraction region ($2\theta = 5$–35°) of polymer matrix to compare crystal structure of PBT. Symbols of (*) and (◆) indicate kaolinite phase in the halloysite and characteristic peak of calcite, respectively. [Color figure can be viewed in the online issue, which is available at wileyonlinelibrary.com.]

the samples given in Figure 3, it can be seen that the characteristic diffraction peaks of crystalline planes of PBT become sharper with higher intensity compared to the extruded PBT. This result clearly indicates that fillers acted crystallization accelerator in the composite samples. It was also observed that all samples crystallized in α-form. Furthermore, crystallite sizes of the samples were determined by the Scherrer equation based on the diffraction pattern;

$$L_{hkl} = \frac{K\lambda}{\beta_{hkl} \cos \theta_{hkl}} \quad (3)$$

where L_{hkl} is the crystallite dimension, or coherence length, perpendicular to the (hkl) plane, K is the Scherrer constant (0.9), and β_{hkl} is the diffraction half-width. First, diffraction patterns of the samples were deconvoluted into five peaks by a Lorentzian function after performing a linear baseline correction in the 2θ range of 10–28°. As an example, deconvoluted patterns of PBT and PBT–HL are compared in Figure 4. Crystallite dimensions of the samples are also listed in Table III. In Figure 4, it is seen that composite sample yielded more intense and sharper peaks than extruded PBT. The diffraction intensities of (010) and (100) crystalline planes are related to the crystal size along the *b*-and *a*-axes. The ratio between the intensities of these crystalline planes also provides information of the crystal growth in the *b*- and *a*-axes directions.[16,17] Refraction of (010) plane is also known to be the preferred growth plane of a lamellae growth direction, as well as (111).[18] It was found that crystallite sizes of the composite samples exhibit a significant increase in 010 plane compared with the PBT. Similarly, crystallite size of 100 plane was found to be slightly increased for the composite samples. But it was also interestingly found that OM enhanced the spherulite size (8.0 nm) compared with the PBT (4.2 nm). This phenomenon can be related with the fact that less effective nucleation effect of organically modified clay layers. Krikorian and Pochan[19] reported the same effect of organo-clay for the isothermal crystallization of poly(L-lactic acid) (PLLA) nanocomposites. They surprisingly observed that exfoliated nanocomposite retarded nucleation but resulted in bigger

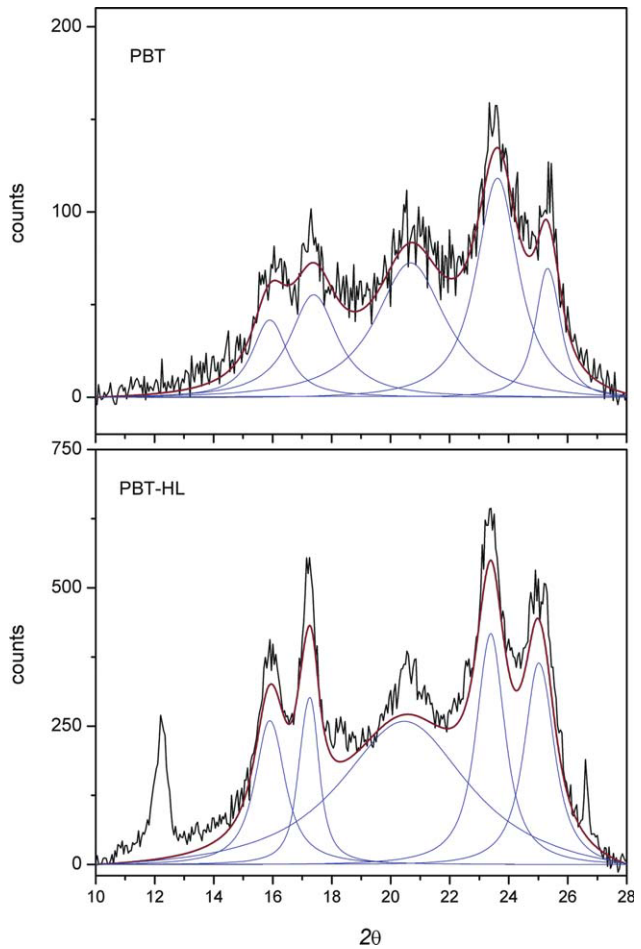

Figure 4 Deconvoluted XRD patterns of the PBT and PBT–HL samples. [Color figure can be viewed in the online issue, which is available at wileyonlinelibrary.com.]

TABLE III
Crystallite Dimensions of PBT and Composite Samples Determined from the Scherrer Equation (nm)

Samples	L_{011}	L_{010}	L_{110}	L_{100}	L_{111}
PBT	5.7	4.2	2.9	4.8	8.2
PBT–CA	6.4	8.7	2.2	6.2	7.4
PBT–HL	6.7	10.3	1.6	7.1	6.9
PBT–OM	6.9	8.0	2.3	5.6	7.3

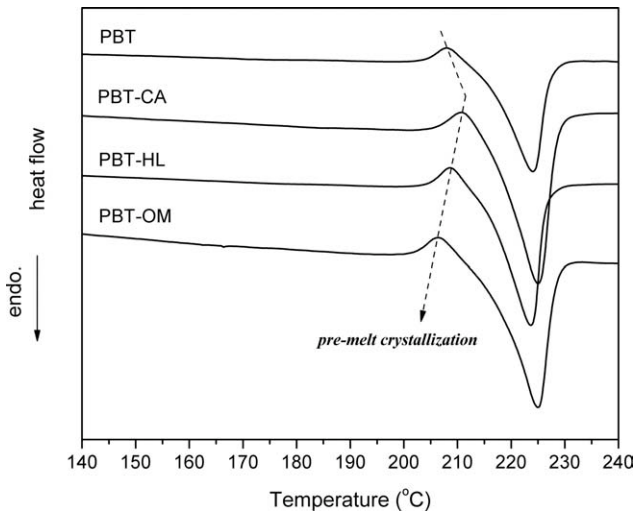

Figure 5 First melting endotherms of the PBT and composite samples recorded at the heating rate of 10°C min^{-1}.

crystals compared with the intercalated sample. Therefore, they entitled their paper as "unusual crystallization behavior." Based on the XRD analysis and kinetic study reported in the present work, XRD analysis and kinetic study are convenient with their findings. Retardation of nucleation due to the presence of organic groups on the filler surfaces means less number of nucleus is occurred at the first stage of crystallization. This could result in more open volume for crystal growing until spherulite impingements. Thus, a growing crystal could geometrically improve even though the growth rate is slow. Consequently, these results indicate that the crystal growth is relatively favored during the crystallization of PBT in the composite samples due to the presence of inorganic fillers. Similar result has been reported before for the isothermally crystallized poly(ethylene terephatalate) (PET)/clay nanocomposites.[20] We also reported that un-modified alumina-silicate layers enhanced the crystallization rate of PET under nonisothermal conditions compared with organically modified counterpart.[21]

Premelt or cold crystallization

Heat flow curves of the PBT and composite samples recorded during the first heating scan at the heating rate of 10°C min^{-1} are given in Figure 5. Premelt-crystallization exotherms as a small shoulder before the melting endotherms observed for all the samples at the heating rate employed. Premelt-crystallization behavior can be attributed to formation of smaller crystals within the amorphous region or re-arrangement of disordered or uncompleted crystals by the chains which gain mobility at the temperatures before melting. It was found that premelt-crystallization peaks of PBT, PBT–CA, PBT–HL, and PBT–OM are 208.0, 210.7, 208.6, and 206.4°C, respectively. It is seen that peak temperature of premelt-crystallization exotherm of PBT–OM is lower than that of PBT and other composite samples. This could be originated from the fact that organic groups between montmorillonite layers enhance the segmental mobility of PBT chains. In our previous study, it has been also observed for the PET/montmorillonite nanocomposites.[21] Similar behavior has been reported for the nonisothermal cold crystallization of PLLA with and without additives.[22,23]

Melt-crystallization kinetics

The crystallization exotherms of PBT and composite samples at various cooling rates are illustrated in Figure 6(a–d). The melt-crystallization onset (T_{co}) and peak temperatures (T_{cp}) of the samples at which the crystallization rate is maximum at all cooling rates are listed in Table IV. As expected, the T_{cp} values shift to lower temperatures with an increasing cooling rate for all the samples. At a given cooling rate, the T_{cp} values of the PBT–CA and PBT–HL samples are higher than that of neat PBT. On the other hand, T_{cp} values of the PBT–OM are lower than that of PBT at all the cooling rates employed. This result refers to deceleration effect of organo-montmorillonite on the crystallization rate of PBT. This effect can be clearly seen in Figure 7. In this figure, crystallization onset temperatures (T_{co}) of the samples are compared for a cooling rate of 5°C min^{-1}. T_{co} value of PBT–OM is lower than those of all samples as well as T_{cp}. This is due to apparently reducing of surface free energy of the alumina-silicate layers by organic modification and therefore, lack of effective nucleating ability of such layers. Similar effect was recently reported for different type of organically surface treated fillers.[24]

This is due to apparently reducing of surface free energy of the alumina-silicate layers by organic modification and therefore, lack of effective nucleating ability of such layers. Figures 8(a-d) and 9(a-d) show the Xc-T and Xc-t plots for the samples, respectively. The most important rate parameter, crystallization half-time ($t_{1/2}$) which is defined as the time taken the crystallinity of the sample reaches the value of 50% of the relative crystallinity, can be obtained from the X_c–t curves. The values of $t_{1/2}$ directly indicate the rate of crystallization process and usually the reciprocal of crystallization half-time ($1/t_{1/2}$, $time^{-1}$) is used to compare crystallization rates of different systems. If $t_{1/2}$ is short or reciprocal half-time is high, it means crystallization is fast. $1/t_{1/2}$ values of the samples at the cooling rates are given in Table IV. Crystallization rates of the samples decrease in the order of PBT–HL > PBT–CA > PBT > PBT–OM. As the samples could have enough

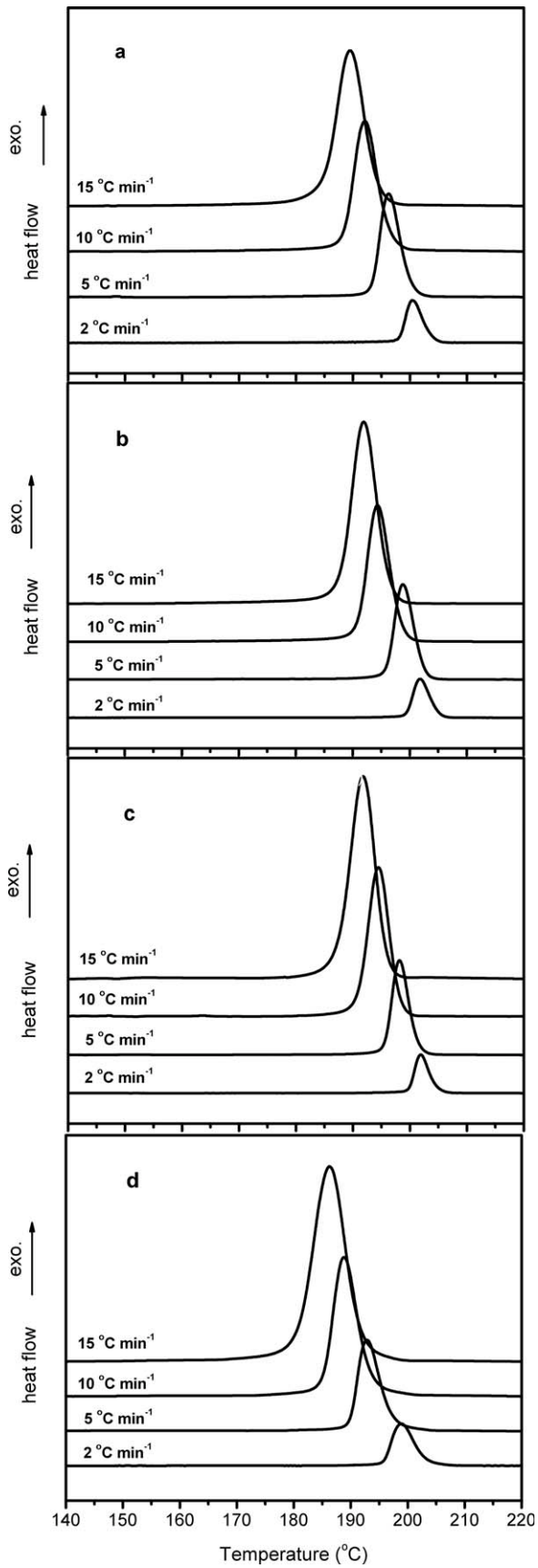

Figure 6 Crystallization exotherms of the samples recorded at various cooling rates, (a) PBT, (b) PBT–CA, (c) PBT–HL, and (d) PBT–OM.

time for proceeding the crystallization at low cooling rates independently from the composition, it is difficult to distinguish variation in crystallization rates of the samples regarding the values of $t_{1/2}$. $1/t_{1/2}$ values of the samples are quite similar at low cooling rate (2°C min^{-1} for the present study). But for the other cooling rates employed, effect of filler type and geometry on the $1/t_{1/2}$ values are obviously seen. Furthermore, one could assume that comparing of $1/t_{1/2}$ values for the higher cooling rates than 15°C min^{-1} might be more significant for the real cooling conditions for the commercial processing operations. It can be inferred that variations in the crystallization rate become more pronounced in the case of real processing and solidification conditions depending on the filler type and geometry. This result implies that PBT composite containing inorganic fillers modified with relatively high amount of organic groups presumably crystallizes lower than a sample having no modifiers.

Enthalpies of melt-crystallization exotherms (ΔH_c), second melting endotherms (ΔH_m), and degree of crystallinity (X_c) values of the samples are also listed in Table IV. As expected, X_c values of the samples decrease with the increasing of cooling rate for all samples. It was found that X_c values of the PBT–HL samples are higher than those of PBT, PBT–CA, and PBT–OM at a particular cooling rate.

Most used kinetic approach for nonisothermal crystallization process of semicrystalline polymers is Ozawa model.[25] It is based on the extended form of Avrami approximation assuming that the nonisothermal crystallization process could be composed of small isothermal steps. Ozawa equation is as follow:

$$\chi_c = 1 - \exp\left(\frac{-K(T)}{\phi^m}\right) \tag{4}$$

where X_c is the relative crystallinity, $K(T)$ is the crystallization rate function, ϕ is the cooling/heating rate (°C min^{-1}), and m is the Ozawa constant depends on the dimension of crystal growth and nucleation mechanism. If double logarithmic form of the equation is taken, a linear relationship is obtained to calculate kinetic constants.

$$\ln[-\ln(1-\chi_c)] = \ln K(T) - m \ln \phi \tag{5}$$

Plotting $\ln[-\ln(1 - \chi_c)]$ against $\ln \phi$ at a given temperature, a straight line should be obtained. Slope of the line is Ozawa constant, m, and intercept of that is $K(T)$. Ozawa plots of the samples are given in Figure 10. As seen in Figure 10, Ozawa model successfully fits the nonisothermal crystallization behavior of the samples, although the model could not be used for modeling of nonisothermal crystallization kinetics of some polymer/clay

TABLE IV
Melt-Crystallization Onset (T_{co}) and Peak (T_{cp}) Temperatures, Crystallization Rates, Enthalpy and Degree of Crystallinity Values of the Samples

Sample	ϕ (°C min^{-1})	T_{co} (°C)	T_{cp} (°C)	$1/t_{1/2}$ (min^{-1})	[a]ΔH_c (J g^{-1})	[b]ΔH_m (J g^{-1})	[c]X_c (%)
PBT	2	203.9	200.4	0.335	33.4	42.2	29.0
	5	200.2	196.3	0.583	50.0	40.6	27.9
	10	196.5	192.1	0.881	49.9	38.9	26.7
	15	194.6	189.5	1.278	37.6	36.6	25.1
PBT–CA	2	205.1	201.8	0.334	38.9	41.0	29.7
	5	202.6	198.8	0.619	44.5	40.8	29.5
	10	198.5	194.3	1.099	38.2	38.4	27.8
	15	196.5	191.9	1.472	39.0	35.2	25.5
PBT–HL	2	204.7	201.9	0.340	34.4	42.8	31.0
	5	201.4	198.2	0.743	39.7	39.4	28.5
	10	198.4	194.5	1.103	51.7	38.3	27.7
	15	195.9	191.8	1.480	42.0	33.9	24.5
PBT–OM	2	203.1	198.9	0.170	49.1	42.7	30.9
	5	197.2	192.9	0.425	45.3	38.3	27.7
	10	193.4	188.8	0.763	38.6	34.4	24.9
	15	191.9	186.3	1.077	33.7	28.3	20.5

[a] Enthalpy of melt-crystallization.
[b] Enthalpy of second melting recorded at the heating rate of 10°C min^{-1}.
[c] Degree of crystallinity calculated from the enthalpy of second melting.

nanocomposite systems.[26,27] Ozawa kinetic parameters are listed in Table V. It was found that Ozawa constant (m) increases with the crystallization temperature up to 197°C. $K(T)$ values are also listed in Table V. It is seen that $K(T)$ values decrease with the increasing of temperature for the PBT and PBT–OM samples. This result suggests that PBT and PBT–OM composites crystallized slower at higher temperatures. But, a correlation between temperature and crystallization rate function [$K(T)$] was not obtained for the PBT–CA and PBT–HL samples. This indicates that crystallization mechanism may differ depending on the undercooling for these samples.

An alternative approach, Avrami model,[28–30] was used in this study to compare crystallization rates of the samples. Avrami equation is as below:

$$\chi_c = 1 - \exp(-Z_t t^n) \tag{6}$$

where n is Avrami constant depending on crystal growth mechanism and Z_t is the rate constant involving both nucleation and growth rate parameters. Avrami model is used to analyze isothermal crystallization kinetics of polymer taking into account of developing relative crystallinity with time. Therefore, it should be noted that in nonisothermal crystallization Avrami kinetic parameters do not have the same physical meanings as in the isothermal crystallization, since the temperature changes steadily in the nonisothermal processes. Both nucleation and crystal growth processes are temperature dependent in the nonisothermal crystallization. However, Avrami model can provide useful insights into the kinetics of nonisothermal crystallization processes. Taking double logarithmic form of eq. (7):

$$\ln[-\ln(1 - \chi_c)] = \ln Z_t + n \ln t \tag{7}$$

and plotting $\ln[-\ln(1 - \chi_c)]$ versus $\ln t$ for each cooling rate, straight line should be obtained to determine kinetic constants. Avrami plots generally fit the experimental data linearly at low degree of

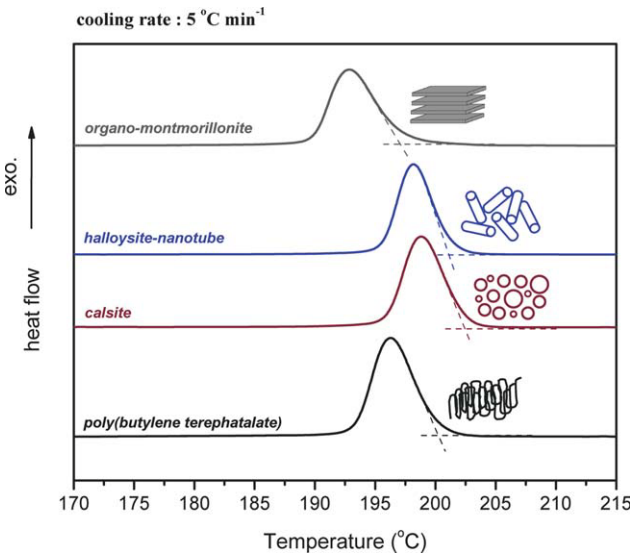

Figure 7 Comparing of crystallization exotherms of the samples depending on the filler geometry. [Color figure can be viewed in the online issue, which is available at wileyonlinelibrary.com.]

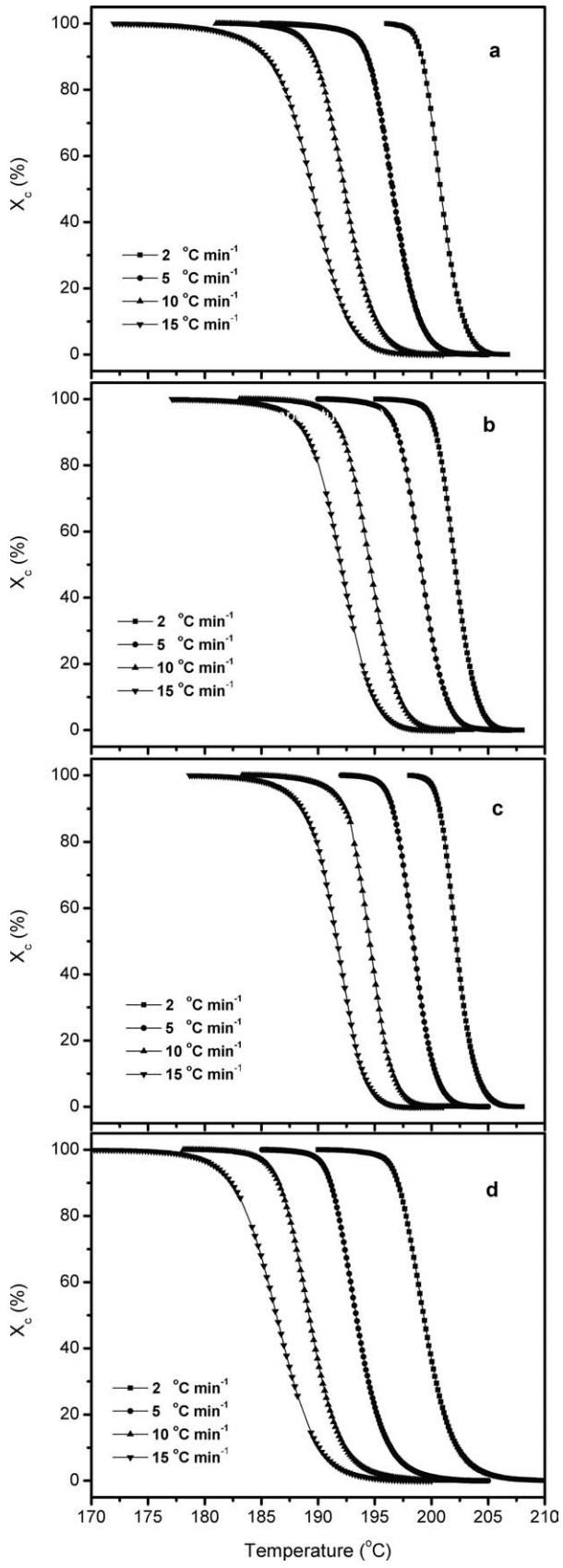

Figure 8 Relative crystallinity (X_c) as a function of temperature (T) at various cooling rates, (a) PBT, (b) PBT–CA, (c) PBT–HL, and (d) PBT–OM.

crystallinity and deviate from the linear regression at higher crystallization ratio as possibly, it does not account the secondary crystallization. In nonisothermal crystallization, temperature change at a given constant cooling rate affects the rate of both nucleation and spherulite growth which are temperature dependent parameters. Considering the temperature dependent character of the nonisothermal crystallization process, the rate parameter, Z_t was modified by Jeziorny.[31]

$$\ln Z_c = \frac{\ln Z_t}{\phi} \tag{8}$$

Avrami plots of the samples were illustrated in Figure 11, and the kinetic constants by Jeziorny modification were listed in Table VI. As shown in Figure 11, Avrami model was able to fit the primary crystallization stage of the samples, and it deviated from the linearity due to the secondary crystallization in all cooling rates. Changes in Avrami constants (n) with cooling rate imply that crystallization of the samples has occurred in various growth forms. It was found that n was in the range of 4.10–7.0 for the PBT, PBT–CA, and PBT–HL samples, whereas it was about 3.0 for the PBT–OM. These results show that heterogeneous nucleation effect of inorganic fillers might be more pronounced for the PBT–CA and PBT–HL samples than PBT–OM. But, n values varied depending on the cooling rate and filler type. Consequently, it is difficult to infer the nucleation mechanism and crystal growth analysis based on the Avrami constants of the samples. On the other hand, crystallization rate parameters (Z_c) of the samples increase with the increasing of cooling rate for all samples. At a given cooling rate, the PBT–HL yielded the highest Z_c values which indicate the fastest crystallization rate. Conversely, the PBT–OM showed the lowest Z_c values.

Another method developed by Liu and Mo[32] was also used to describe the nonisothermal melt-crystallization process. Liu et al. offered a new method combining the Avrami and Ozawa equations at a given value of X_c as follows:

$$\ln K(T) - m \ln \phi = \ln Z_t + n \ln t \tag{9}$$

$$\ln \phi = \ln F(T) - a \ln t \tag{10}$$

where the parameter $F(T) = [K(T)/Z_t]^{1/m}$ refers to the cooling rate and a is the ratio of the Avrami constant n, to the Ozawa constant m. According to Liu model, plotting ln ϕ versus ln t, series of straight lines are obtained at a given value of relative crystallinity. The kinetic parameters, $F(T)$ and a, could be determined by intercept and slope of these lines, respectively. At a certain value of relative

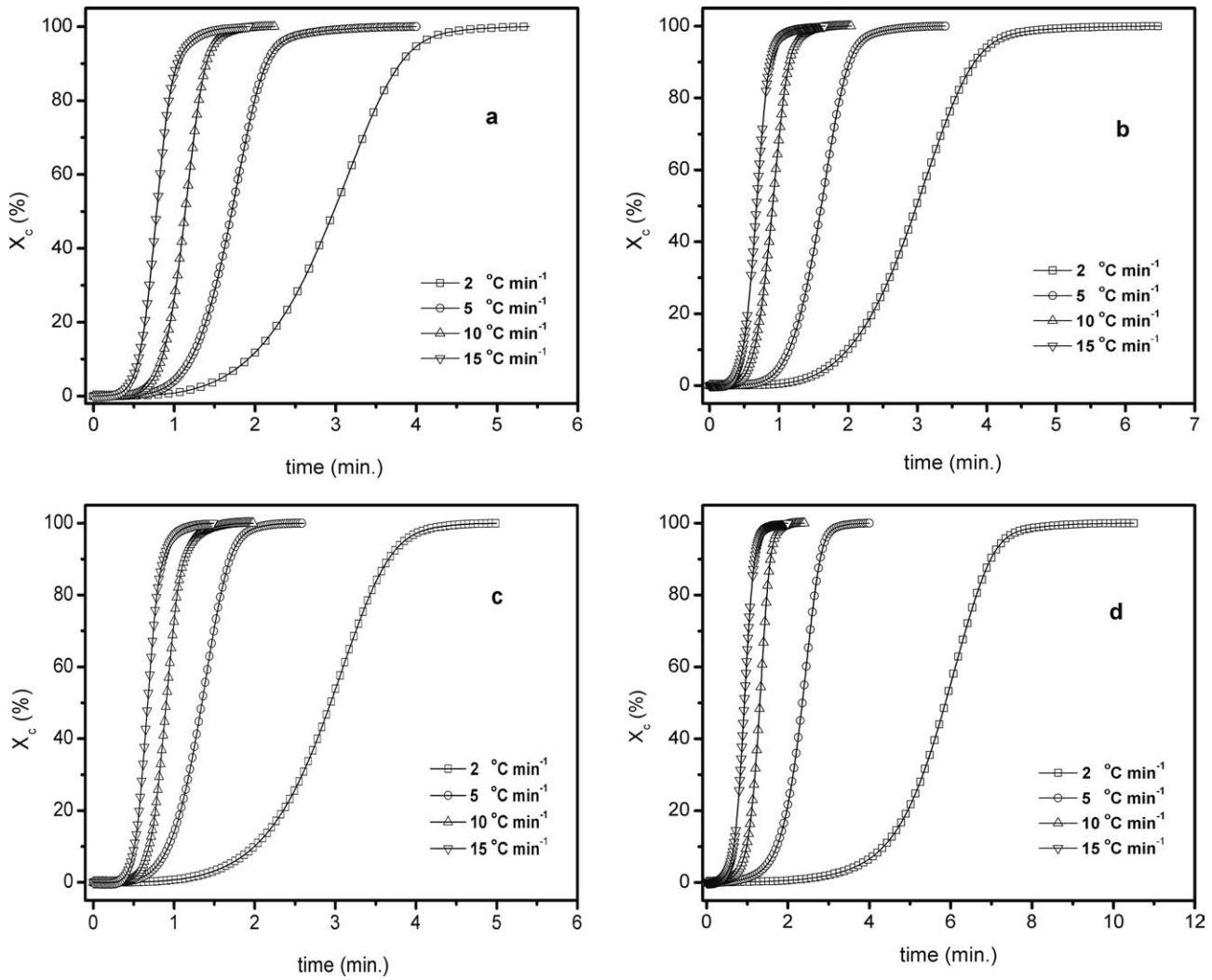

Figure 9 Relative crystallinity (X_c) as a function of time (t) at various cooling rates, (a) PBT, (b) PBT–CA, (c) PBT–HL, and (d) PBT–OM.

crystallinity, X_c, higher value of $F(T)$ means that high cooling rate is needed to reach this X_c in a unit time which also indicates the difficulty in crystallization process.

Liu-Mo model was applied to the samples at the relative crystallinity values of 20%, 40%, 60%, and 80%. Table VII summarizes the values of Liu-Mo parameters for the samples. As shown in Figure 12, Liu-Mo model was successful to fit the crystallization kinetics of the PBT and composites. Values of a increased with the increasing of relative crystallinity for the PBT–OM, whereas those values decreased with the increasing of X_c for the other samples. This implies that crystallization mechanism varies by the presence of organically modified inorganic filler within the PBT phase. In Table VII, it can be seen that $F(T)$ values increase with the developing of X_c. From Liu-Mo modeling of the samples, $F(T)$ values of PBT are higher than those of PBT–CA and PBT–HL samples. It was found that the PBT–OM yielded the highest $F(T)$ values at a given relative crystallinity value. This indicates that organic groups between the clay layers decelerate the crystallization. Our results are consistent with the reported kinetic data for the crystallization of PET/clay nanocomposites. Chung et al.[33] studied nonisothermal crystallization behavior of exfoliated PET/layered silicate nanocomposites prepared by solution mixing method. They examined the effects of organic modifier onto clay layers on the crystallization of PET by DSC method. They found that PET nanocomposites had shorter crystallization half-times than PET because of dispersed silicate layers, which acted as a nucleating agents. In their study, it was also reported that PET nanocomposite excluding organic modifier by solvent–nonsolvent system showed higher crystallization rate than the nanocomposite including organic modifier. Based on this result, they

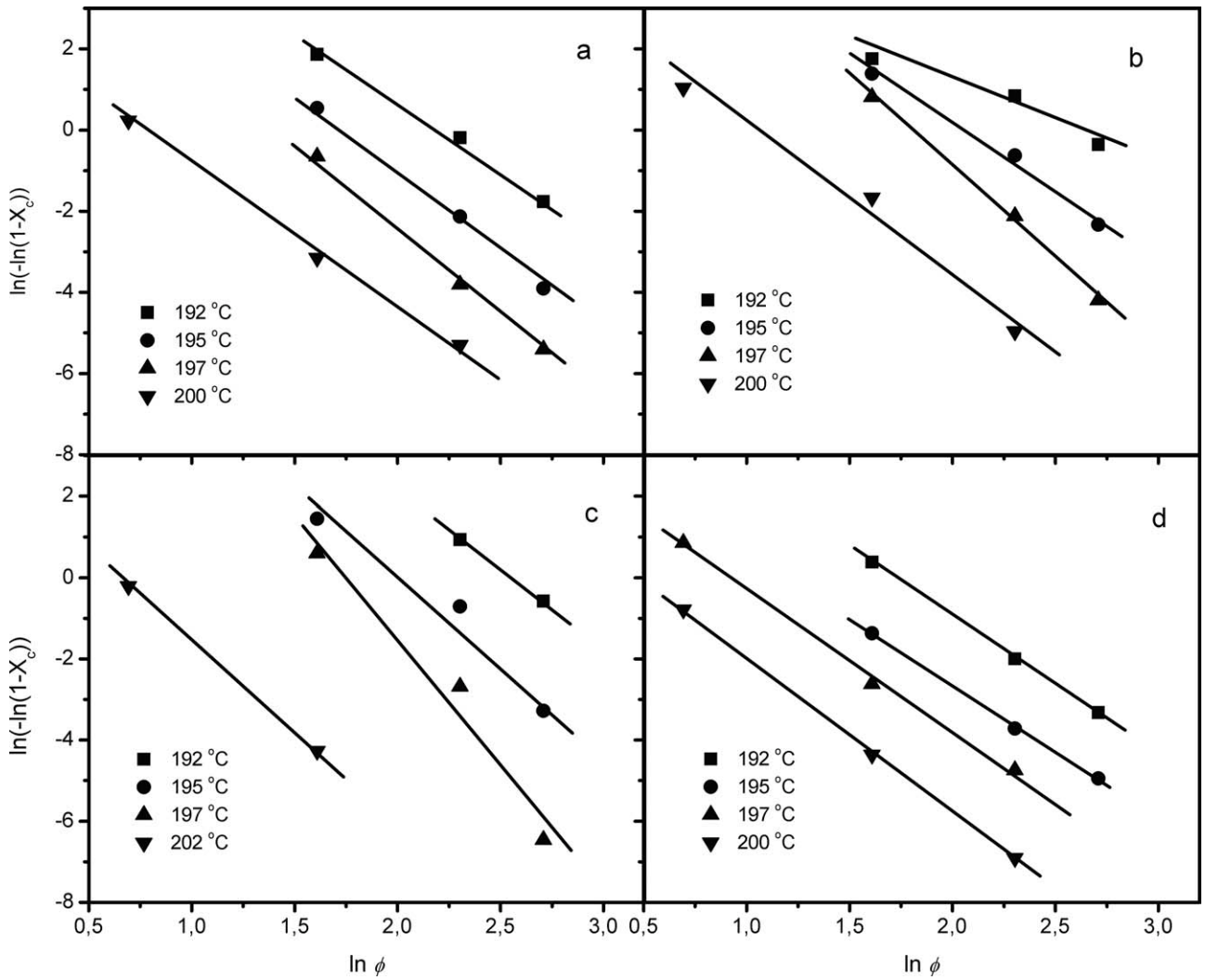

Figure 10 Ozawa plots of the samples, (a) PBT, (b) PBT–CA, (c) PBT–HL, and (d) PBT–OM.

have concluded that organic groups physically hinder the packaging of the PET chains in regular manner and interrupt the lamellar pathway. In our previous study, it was also shown that organic groups between clay layers make the crystallization difficult because of possibly decelerating nucleation by reducing the surface free energy of filler surfaces and hindering the packaging of PET chains and slowing the chain transfer toward the developing crystal face during the crystal growth.[21]

Another simple and quantitative approach for comparing effects of fillers on the nonisothermal crystallization rate of the samples is to calculate the crystallization rate parameter (CRP) which can be determined slope of a linear plot of $1/t_{1/2}$ versus the cooling rate (ϕ).[34,35] Figure 13 shows the plots of $1/t_{1/2}$ versus cooling rate for the samples. The values of CRP were found to be 0.071, 0.088, 0.085, and 0.069 for the PBT, PBT–CA, PBT–HL, and PBT–OM, respectively. The higher CRP values for the PBT–CA and PBT–HL indicate that CA and HL effectively enhanced the crystallization of the PBT. On the other hand, CRP value of the PBT–OM sample refers that organo-montmorillonite impeded the crystallization due to the presence of

TABLE V
Ozawa Kinetic Parameters

Sample	Temperature (°C)	m	$K(T)$ [(°C min^{-1})^m]	r^2
PBT	192	3.26	7.23	0.997
	195	4.02	7.04	0.999
	197	4.34	6.30	0.999
	200	3.45	2.56	0.998
PBT–CA	192	1.86	4.85	0.974
	195	3.33	6.82	0.995
	197	4.52	8.15	0.998
	200	3.71	3.70	0.998
PBT–HL	192	3.73	9.54	0.999
	195	4.17	8.36	0.980
	197	6.24	10.92	0.982
	202	4.43	2.87	0.999
PBT–OM	192	3.38	5.82	0.999
	195	3.26	3.86	0.999
	197	3.49	3.20	0.998
	200	3.80	1.83	0.999

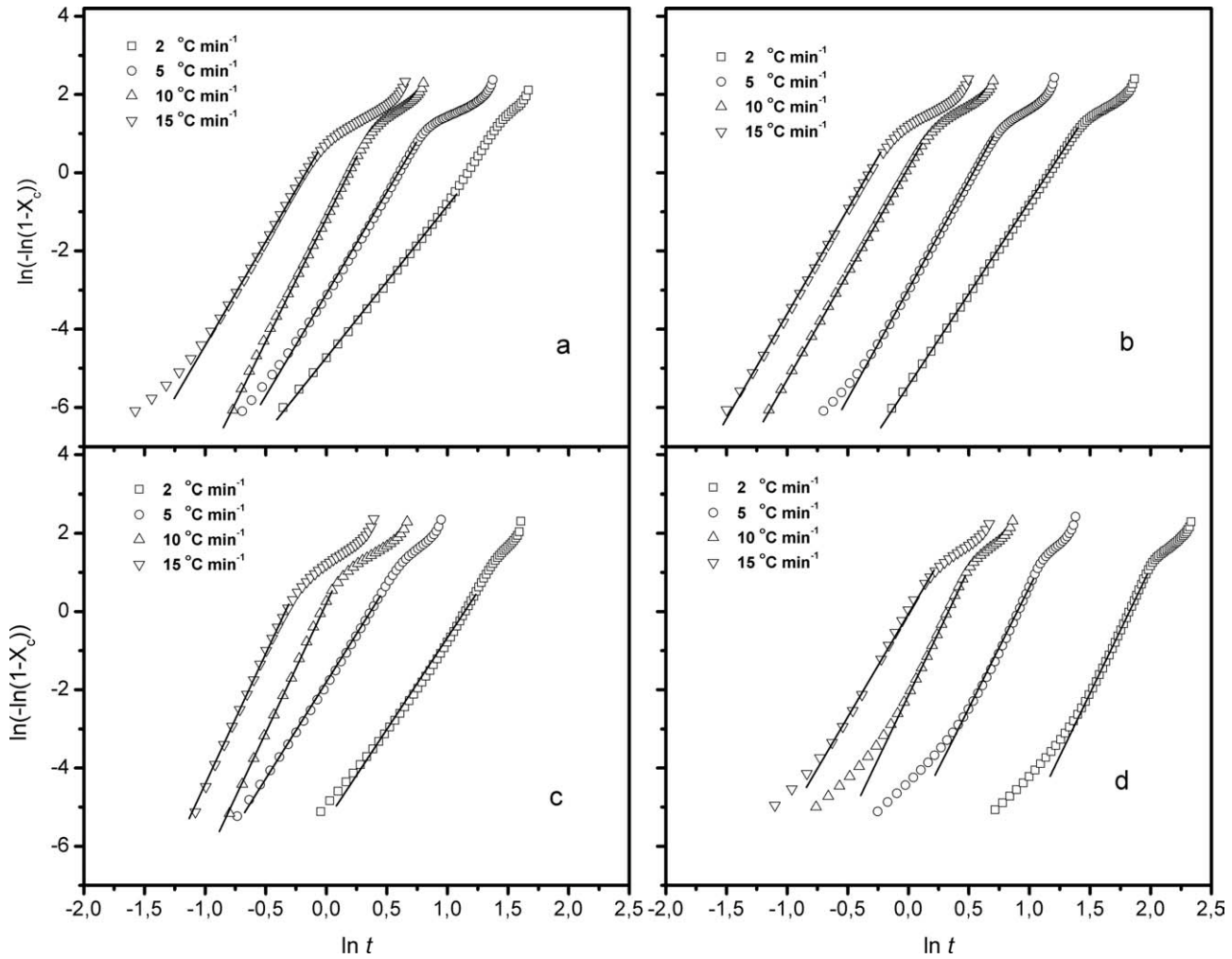

Figure 11 Avrami plots of the samples, (a) PBT, (b) PBT–CA, (c) PBT–HL, and (d) PBT–OM.

organic groups. This result is convenient with the kinetic findings mentioned above.

Nucleation activity of fillers

Dobreva and Gutzow[36,37] suggested a simple method to calculate the nucleation activity of foreign substrates, additives, etc. in a polymer melt. This method has also been used for silica nanoparticle-filled PEN,[38] surface-modified talc-polypropylene (PP) composites,[39] and PP/SiO_2 nanocomposites.[40] Nucleation activity (φ) can be defined as a factor by which the work of three-dimensional nucleation decreases with the addition of a foreign substrate. If the foreign substrate is extremely active for nucleation, value of φ approaches 0, whereas it is about 1 for inert particles. Mathematically, the nucleation activity is the ratio of B parameters in heterogeneous and homogenous medium;

$$\varphi = \frac{B^*}{B} \tag{11}$$

B parameter is defined as;

$$B = \frac{\omega\sigma^3 V_m^2}{3nk_B T_m^0 \Delta S_m^2} \tag{12}$$

TABLE VI
Avrami–Jeziorny Kinetic Parameters

Sample	ϕ (°C min^{-1})	n	Z_c (min^{-1})	r^2
PBT	2	4.10	0.08	0.9987
	5	4.74	0.55	0.9977
	10	5.95	0.88	0.9987
	15	4.98	1.05	0.9986
PBT–CA	2	4.54	0.07	0.9999
	5	5.53	0.54	0.9997
	10	5.41	1.01	0.9999
	15	5.39	1.12	0.9985
PBT–HL	2	4.27	0.09	0.9973
	5	4.77	0.69	0.9998
	10	6.82	1.03	0.9996
	15	6.96	1.18	0.9994
PBT–OM	2	2.84	0.03	0.9952
	5	2.92	0.42	0.9995
	10	2.96	0.76	0.9981
	15	3.02	0.90	0.9977

TABLE VII
Liu-Mo Kinetic Parameters and Crystallization Activation Energies of the Samples

				ΔE_A (kJ mol^{-1})		
Sample	X_c (%)	a	ln $F(T)$	Kissinger	Takhor	Augis–Bennett
PBT	20	1.60	2.10	−341.8	−334.0	−284.4
	40	1.55	2.32			
	60	1.54	2.49			
	80	1.53	2.65			
PBT–CA	20	1.37	1.91	−367.3	−359.0	−306.6
	40	1.35	2.12			
	60	1.34	2.26			
	80	1.34	2.41			
PBT–HL	20	1.43	1.87	−373.6	−365.5	−312.8
	40	1.38	2.06			
	60	1.37	2.19			
	80	1.37	2.33			
PBT–OM	20	1.07	2.38	−296.8	−289.3	−243.0
	40	1.09	2.55			
	60	1.09	2.64			
	80	1.11	2.76			

where ω is a geometric factor, σ is a specific energy, V_m is the molar volume of the crystallizing substance, n is the Avrami exponent, ΔS_m is the melting entropy, and T_m^0 the equilibrium melting temperature.

However, B parameter could be determined experimentally by using the simple definitions of nonisothermal crystallization. For homogenous nucleation, B parameter can be calculated from the following equation:

$$\ln \phi = C - \frac{B}{\Delta T_c^2} \tag{13}$$

where ϕ is the cooling rate, C is a constant, and ΔT_c is the supercooling ($T_m - T_c$). For heterogeneous nucleation eq. (14) becomes:

$$\ln \phi = C - \frac{B^*}{\Delta T_c^2} \tag{14}$$

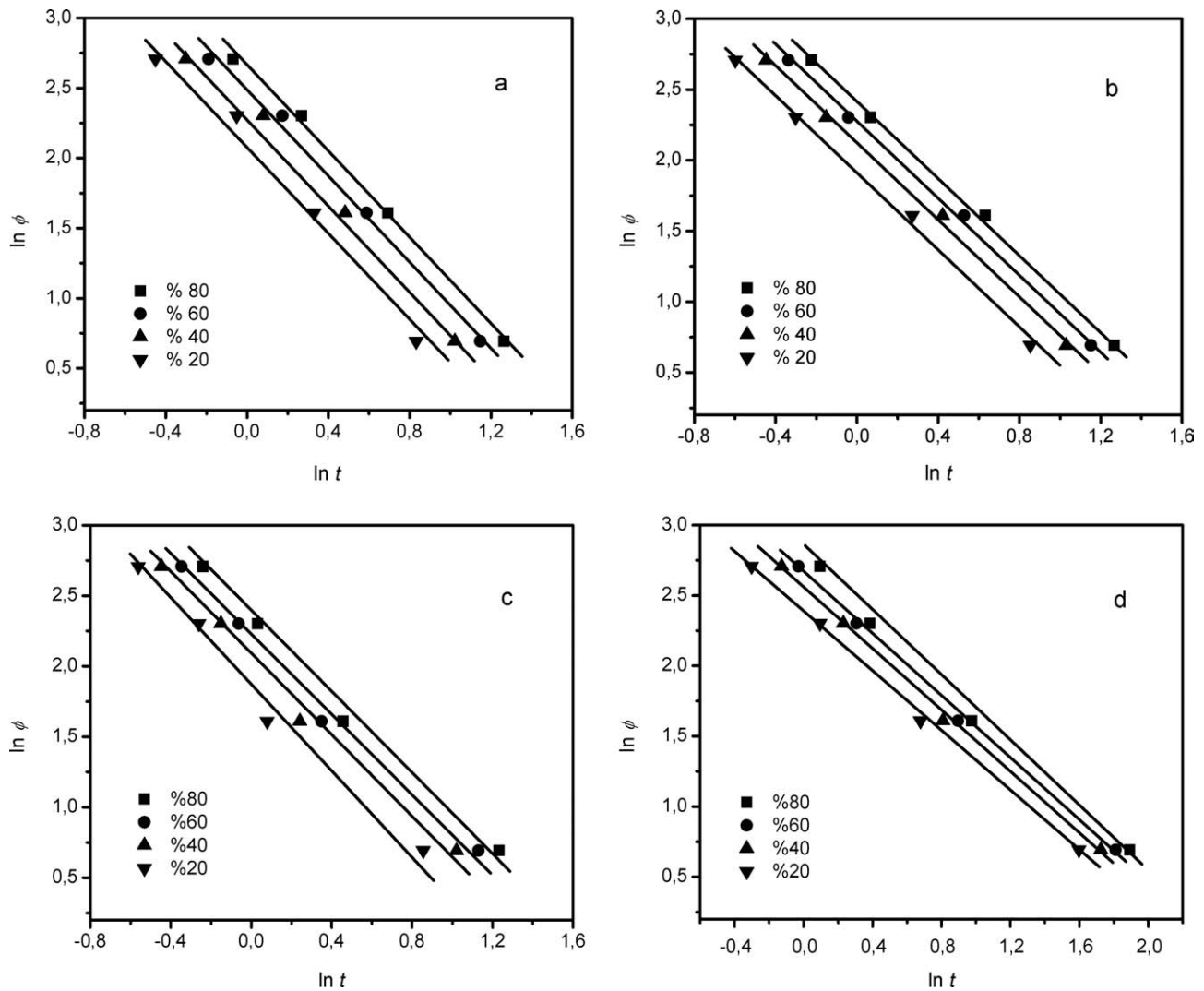

Figure 12 Liu-Mo plots of the samples, (a) PBT, (b) PBT–CA, (c) PBT–HL, and (d) PBT–OM.

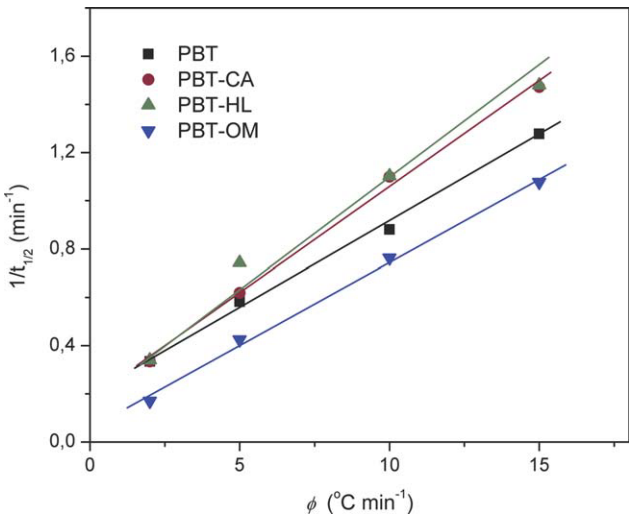

Figure 13 Plots of reciprocal crystallization half-time as a function of cooling rate for the samples. [Color figure can be viewed in the online issue, which is available at wileyonlinelibrary.com.]

B and/or B^* can be obtained by plotting ln ϕ versus the $1/\Delta T_c^2$. These plots of the samples are given in Figure 14. From the calculation, B^* values were found to be 0.897, 0.896, and 0.970 for the PBT–CA, PBT–HL, and PBT–OM samples, respectively. The PBT–OM yielded higher B^* value than the PBT–CA and PBT–HL, whereas almost the same values of B^* were obtained for the CA and HL filled samples. It is also interesting that the B^* value of PBT–OM is slightly lower than unit which refers to inert particle criteria for the nucleation. It can be concluded that organic groups blocking the nucleation activity of inorganic structure by covering up the alumina-silicate layers. Papageorgiou et al.[40] reported that the B^* value were 0.917 ± 0.069 for the 2.5 wt % organo-silane treated silica (particle size of 12 nm and specific surface area of 170 m^2 g^{-1}) filled PP nanocomposite. But, Alonso et al.[39] calculated the nucleation activity value as 0.45 for the %2 organo-silane treated talc containing PP composite. Considering reported values, it could be pointed out that fillers having no or very little amount of organic modifiers act more active nucleators than the counterparts including relatively high amount of organic groups. It can be deduced that the surface character of a filler, which particularly refers to surface free energy, is also decretive on the nucleation as well as particle size and geometry. Based on our results, it is difficult to conclude effect of filler geometry (1D, 2D, and 3D) on the nucleation activity of various types of particles for the nonisothermal melt-crystallization of PBT.

Activation energy for melt-crystallization

Several mathematical models have been proposed to calculate activation energy of the crystallization process. In this study, the Kissinger,[41] Takhor,[42] and Augis and Bennett[43] methods were used. These methods are based on the finite relationship between the peak temperatures T_c obtained from the nonisothermal crystallization exotherms and the heating/cooling rates used.

Kissinger [eq. (16)], Takhor [eq. (17)], and Augis–Bennett [eq. 18)] equations can be described as follows:

$$\frac{d\left[\ln\left(\frac{\phi}{T_c^2}\right)\right]}{d\left[\frac{1}{T_c}\right]} = -\frac{\Delta E_A}{R} \tag{15}$$

$$\frac{d[\ln(\phi)]}{d\left[\frac{1}{T_c}\right]} = -\frac{\Delta E_A}{R} \tag{16}$$

$$\frac{d\left[\ln\left(\frac{\phi}{T_o - T_c}\right)\right]}{d\left[\frac{1}{T_c}\right]} = -\frac{\Delta E_A}{R} \tag{17}$$

where ϕ is the cooling rate (°C min^{-1}), T_c is the crystallization peak temperature (K), T_o is an initial temperature which is taken 232°C for PBT and composite samples, ΔE_A is the activation energy of crystallization process (kJ mol^{-1}), and R is the universal gas constant (8.314 kJ mol^{-1} K^{-1}). In each model, when the parameter of $\ln(\phi/T_c^2)$ or $\ln(\phi)$ or $\ln(\phi/(T_o - T_c)$ is plotted against $1/T_c$, slope of the curve gives activation energy of the process. Kissinger, Takhor, and Augis–Bennett plots of the samples are given in Figures 15(a–c), ΔE_A values are listed in Table VII. ΔE_A is negative due to exothermic nature of the transition from melt to crystalline state and negative activation energy values also imply that

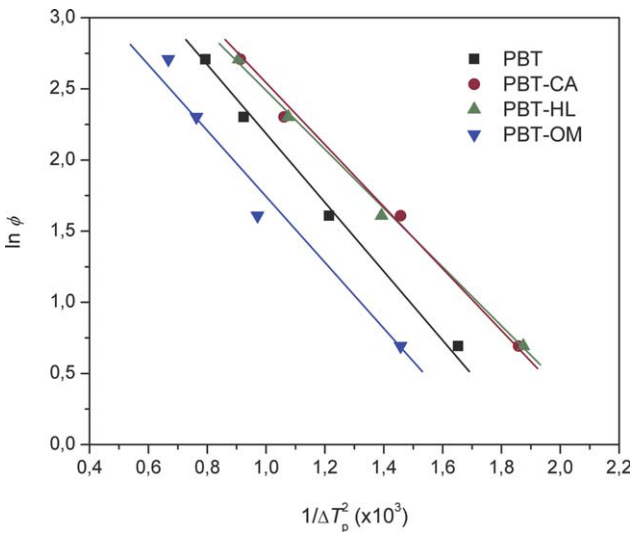

Figure 14 Nucleation activity plots of the samples. [Color figure can be viewed in the online issue, which is available at wileyonlinelibrary.com.]

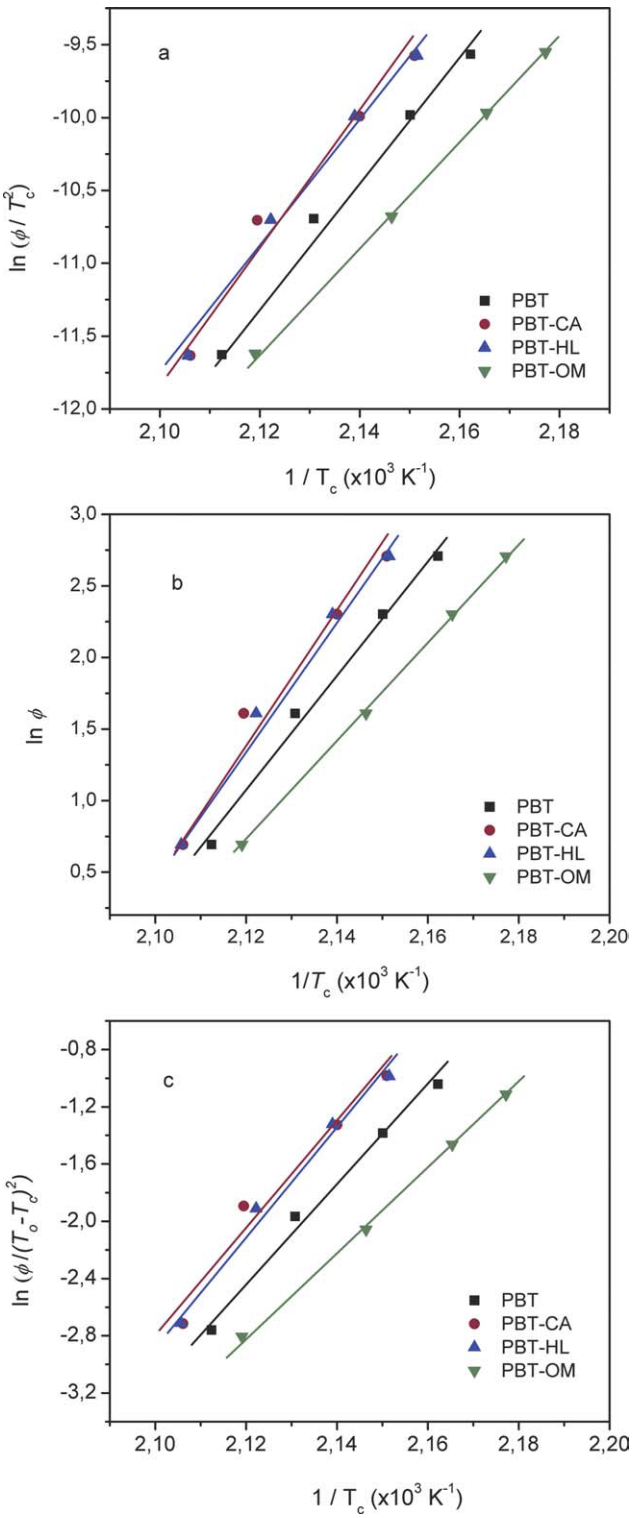

Figure 15 Kissinger (a), Takhor (b), and Augis–Bennett (c) plots of the samples. [Color figure can be viewed in the online issue, which is available at wileyonlinelibrary.com.]

crystallization mechanisms are accelerated by decreasing the temperatures. Negative activation energy values have been reported for nonisothermal crystallization of PBT/clay nanocomposite systems.[14] But, in the literature, an obvious disagreement has been attracted to conclude activation energy values for the heterogeneously crystallized systems. Some authors have reported the ΔE_A values as negative, whereas some others only compared with absolute values. Huang[44] calculated the dependence of effective activation energy on conversion and temperature by Friedman method for the nonisothermal crystallization of PBT/clay nanocomposites. He found that at lower X_c, the PBT/clay nanocomposites showed lower activation energy than neat PBT; however, at higher X_c, nanocomposites exhibited higher activation energy. In this study, it is seen that the Augis–Bennett model yielded lower ΔE_A values than the Kissinger and Takhor models, but the same trend were observed in all approaches employed depending on the compositional variation. It was found that the PBT–OM exhibits the highest ΔE_A value compared with neat PBT and composite samples. This result indicates that energy barrier for the melt-crystallization of organo-montmorillonite containing sample is higher than the neat PBT and composite samples including CA and HL as filler. It was also found that ΔE_A values of PBT–CA and PBT–HL were lower than PBT which refers to CA and halloysite act as nucleating agents by lowering the crystallization activation energy. Wang et al.[45] reported higher ΔE_A values for the PET/clay nanocomposites having 1.5 wt % of clay than neat PET and concluded that introduction of clay into PET matrix weakens the dependence of the nonisothermal crystallization exotherms peak temperatures (T_{cp}) on the cooling rates (ϕ).

CONCLUSIONS

The melt-crystallization behavior of PBT and PBT-based composites prepared by melt processing and including 5 wt % of different types of filler, HL (tubular alumina-silicate as 1D filler), organo-montmorillonite (organically modified layered alumina-silicate as 2D filler), and CA (spherical $CaCO_3$ particles as 3D filler), were studied. By comparing effect of filler type on the melt-crystallization kinetics of PBT, it was found that the HL and CA enhanced the crystallization rate of polymer matrix. In case of 1D and 3D fillers, this enhancement in the crystallization rate could be explained by the fact that geometrically less efficient restriction effect of such fillers on the polymer chains compared with the platelet-like, 2D layered filler which has considerably high surface area during the crystal growth step. DSC studies revealed that organic modifier between the clay layers inhibited the crystallization because of physically hindering the packaging of PBT chains and slowing the chain transfer toward the developing crystal face. Based on the kinetic study, it can be also concluded

that surface character of a filler which refers to organic modification and depending polymer-filler interactions are important on the crystallization behavior of polymer composites as well as the particle size, geometry and dispersion. PBT is one of the most widely used thermoplastic polyester as injection molded parts in many types of equipment of electrical devices and automotive parts. Thus it requires a fast molding cycle for the high production rates in plastic industry. On the other hand, for many semicrystalline thermoplastics, preparing of nanocomposites loaded with several types of nanosize fillers (mainly organo-clays) is still rapidly growing research area to improve innovative composite materials in plastic industry. This study shows the fact that introducing organically modified alumina-silicate into the PBT-based composites could reduce the production rate of the parts during the industrial polymer processing operation, especially injection molding.

The authors thank Advansa, TR for supplying the PBT and Mikron'S, TR for supplying the calcite used in this work.

References

1. Yokouchi, M.; Sakakibara, Y.; Chatani, Y.; Tadokoro, H.; Tanaka, T.; Yoda, K. Macromolecules 1976, 9, 266.
2. García-Gutiérrez, M. C.; Hernández, J. J.; Nogales, A.; Panine, P.; Rueda, D. R.; Ezquerra, T. A. Macromolecules 2008, 41, 844.
3. Hernández, J. J.; García-Gutiérrez, M. C.; Nogales, A.; Rueda, D. R.; Ezquerra; T. A. Macromolecules 2009, 42, 4374.
4. Li, G. J.; Fan, S. R.; Wang, K.; Ren, X. L.; Mu, X. W. Iran Polym J 2010, 19, 115.
5. Park, C. S.; Lee, K. J.; Kim, S. W.; Lee, Y. K.; Nam, J. D. J Appl Polym Sci 2002, 86, 478.
6. Jang, S. H.; Kim, Y. H.; Lim, S.; Choi, G. D.; Kim, S. H.; Kim, W. H. J Appl Polym Sci 2010, 116, 3005.
7. Chang, J. H.; Mun, M. K.; Kim, J. C. J Appl Polym Sci 2007, 106, 1248.
8. Pillin, I.; Pimbert, S.; Feller, J. F.; Levesque, G. Polymer Eng Sci 2001, 41, 178.
9. Gallagher, K. P.; Zhang, X.; Runt, J. P.; Huynh-Ba, G.; Lin, J. S. Macromolecules 1993, 26, 588.
10. Tomar, N.; Maiti, S. N. J Appl Polym Sci 2009, 113, 1657.
11. Kim, J. Y. J Appl Polym Sci 2009, 112, 2589.
12. Wu, D.; Zhou, C.; Fan, X.; Mao, D.; Bian, Z. J Appl Polym Sci 2006, 99, 3257.
13. Chen, X.; Xu, J.; Lu, H.; Yang, Y. J Polymer Sci B: Polymer Phys 2006, 44, 2112.
14. Al-Mulla, A.; Mathew, J.; Yeh, S. K.; Gupta, R. Compos A: Appl Sci Manuf 2008, 39, 204.
15. Righetti, M. C.; Di Lorenzo, M. L.; Angiuli, M.; Tombari, E.; La Pietra, P. Eur Polymer J 2007, 43, 4726.
16. Li, X.; Guo, W.; Wu, C. J Macromol Sci B: Phys 2007, 46, 761.
17. Murthy, N. S.; Correale, S. T.; Minor, H. Macromolecules 1991, 24, 1185.
18. Geil, P. H. Polymer Single Crystals; Interscience: New York, 1963.
19. Krikorian, V.; Pochan, D. J Macromol 2004, 37, 6480.
20. Wan, T.; Chen, L.; Chua, Y. C.; Lu, X. J Appl Polym Sci 2004, 94, 1381.
21. Durmus, A.; Ercan, N.; Soyubol, G.; Deligöz, H.; Kaşgöz, A. Polymer Compos 2010, 31, 1056.
22. Tsuji, H.; Takai, H.; Fukuda, N.; Takikawa, H. Macromol Mater Eng 2006, 291, 325.
23. Mano, J. F.; Wang, Y.; Viana, J. C.; Denchev, Z; Oliveira, M. J. Macromol Mater Eng 2004, 289, 910.
24. Deshmukh, D. S.; Pathak, D. U.; Peshwe, D. R.; Ekhe, J. D. Bull Mater Sci 2010, 33, 277.
25. Ozawa, T. Polymer 1971, 12, 150.
26. Xu, W.; Ge, M.; He, P. J Polym Sci B: Polymer Phys 2002, 40, 408.
27. Xu, W.; Zhai, H.; Guo, H.; Whitely, N.; Pan, W. P. J Therm Anal Calorim 2004, 78, 101.
28. Avrami, M. J Chem Phys 1939, 7, 1103.
29. Avrami, M. J Chem Phys 1940, 8, 212.
30. Avrami, M. J Chem Phys 1941, 9, 177.
31. Jeziorny, A. Polymer 1978, 19, 1142.
32. An, Y.; Dong, L.; Mo, Z.; Liu, T.; Feng, Z. J Macromol Sci B: Phys 1998, 36, 1305.
33. Chung, J. W.; Son, S. B.; Chun, S. W.; Kang, T. J.; Kwak, S. Y. Polymer Degrad Stabil 2008, 93, 252.
34. Zhang, U.; Zheng, H.; Lou, X.; Ma, D. J Appl Polym Sci 1994, 51, 51.
35. Supaphol, P.; Dangseeyun, N.; Simoon, P. Polymer Test 2004, 23, 175.
36. Dobreva, A.; Gutzow, I. J Non-Cryst Solids 1993, 62, 1.
37. Dobreva, A.; Gutzow, I. J Non-Cryst Solids 1993, 62, 13.
38. Kim, S. H.; Ahn, S. H.; Hirai, T. Polymer 2003, 44, 5625.
39. Alonso, M.; Velasco, J. I.; De Saja, J. A. Eur Polymer J 1997, 33, 255.
40. Papageorgiou, G. Z.; Achilias, D. S.; Bikiaris, D. N.; Karayannidis, G. P. Thermochim Acta 2005, 427, 117.
41. Kissinger, H. E. J Res Natl Bur Stand 1956, 57, 217.
42. Takhor, R. L. Adv in Nucleation and Crystallization of Glasses; American Ceramic Society: Columbus, 1971; p 166.
43. Augis, J.; Bennett, J. E. Thermochim Acta 1978, 13, 283.
44. Huang, J. W. J Polym Sci B: Polymer Phys 2008, 46, 564.
45. Wang, Y.; Shen, C.; Li, H.; Li, Q.; Chen, J. J Appl Polym Sci 2004, 91, 308.